Structural studies of the binding of an antagonistic cyclic peptide to the VEGFR1 domain 2

Lei Wang, Pascale Coric, Sylvain Broussy, Rossella Di Stasi, Lingyu Zhou, Luca d'Andrea, Lili Ji, Michel Vidal, Serge Bouaziz, Wang-Qing Liu

Structural studies of the binding of an antagonistic cyclic peptide to the VEGFR1 domain 2

Lei Wang,[†,1,2] Pascale Coric,[§,1] Sylvain Broussy,[†] Rossella Di Stasi,[‡] Lingyu Zhou,[#] Luca D. D'Andrea,[‡] Lili Ji,[#] Michel Vidal,[†,∞] Serge Bouaziz,[*,§] and Wang-Qing Liu[*,†]

[†] UMR 8038 CNRS, U 1268 INSERM, Faculté de Pharmacie de Paris, Université Paris Descartes, Sorbonne Paris Cité, 4 avenue de l'Observatoire, Paris 75006, France.

[§] UMR 8038 CNRS, Faculté de Pharmacie de Paris, Université Paris Descartes, Sorbonne Paris Cité, 4 avenue de l'Observatoire, Paris 75006, France.

[‡] Istituto di Biostrutture e Bioimmagini, CNR, via Mezzocannone 16, 80134 Napoli, Italy.

[#] The MOE Key Laboratory for Standardization of Chinese Medicines, Shanghai Key Laboratory of Compound Chinese Medicines, Institute of Chinese Materia Medica, Shanghai University of Traditional Chinese Medicine, 1200 Cailun Road, Shanghai 201203, China.

[∞] UF biologie du médicament, toxicologie, hôpital Cochin, AP-HP, 27 rue du Faubourg Saint Jacques, Paris 75014, France.

***Correspondence should be addressed to:**

Serge Bouaziz (serge.bouaziz@parisdescartes.fr; tel. +33.(0)1 53 73 97 04)

Wang-Qing Liu (wangqing.liu@parisdescartes.fr; tel. +33.(0)1 53 73 15 65)

[1] These authors contributed equally to this study.
[2] Present address: College of Life Science, Zhejiang Sci-Tech University, Hangzhou 310018, P. R. China.

ABSTRACT

Physiological and pathological angiogenesis is mainly regulated by the binding of the vascular endothelial growth factor (VEGF) to its receptors (VEGFRs). Antagonists of VEGFR are very attractive for the treatment of diseases related to excessive angiogenesis. Our previously designed C-terminal alkylated cyclic peptides [YKDEGLEE]-NHR (R = alkyl, arylalkyl) disrupt the interaction between VEGF and VEGFRs in biological assays. In this paper, we described the structural studies of the binding of one of these cyclic peptides named Peptide **3** to the VEGFR1 domain 2 (VEGFR1-D2). The molecular docking and NMR mapping identified the binding site on VEGFR1-D2. The anti-angiogenic effect of our peptide was evaluated by an experiment of VEGF-induced tube formation in two cell lines, retinal cell type RF6/A and vascular endothelial cell type HUVEC. Some new peptides were also synthesized and compared by an ELISA-based assay, in order to verify their ability to disrupt the formation of the complex VEGF-A/VEGFR1. In conclusion, the structural studies of Peptide **3** with VEGFR1-D2 will help the design of more efficient VEGFR antagonist. Moreover, Peptide **3**, with improved receptor binding affinity, could be more suitable for VEGFR targeting bioimaging studies once labelled.

Keywords: angiogenesis; VEGF; VEGFR; cyclic peptide; NMR mapping.

1. INTRODUCTION

Angiogenesis, the formation of new blood vessels from preexisting vasculature, is a fundamental physiological process during fetal development and tissue repair [1,2]. The process is tightly regulated by pro- and anti-angiogenic factors. Abnormal angiogenesis is involved in various pathological disorders, including vascular insufficiency (myocardial infarction, limb ischemia and arteriosclerosis) and vascular overgrowth (hemangiomas, retinopathies, and vascularized tumors) [3-5]. Angiogenesis is mediated by the effectors belonging to the vascular endothelial growth factor family (VEGF-A, B, C, D and PlGF (placental growth factor)), among which, VEGF-A (usually named VEGF) represents as the most effective isoform [6].

VEGF-A is a dimeric glycoprotein that exerts its pro-angiogenic effects through the binding to three structurally related tyrosine kinase receptors (VEGFR1, VEGFR2 and VEGFR3) [7] and two co-receptors, neuropilins 1 and 2 (NRP1 and NRP2), lacking cytosolic catalytic activity [8]. While VEGFR1, VEGFR2 and NRP1 are implicated in angiogenesis, VEGFR3 and NRP2 are predominantly involved in lymphangiogenesis. Blocking the interaction between VEGF and its receptors for therapeutic and diagnostic purposes has been an intense research subject during the past decades, leading nowadays to clinic treatments [9].

The molecules able to block the interaction between VEGF and its receptors are called antiangiogenic agents or antagonists. They can interfere with angiogenesis in various manners. Antibodies that specifically bind to VEGF (bevacizumab) or VEGFRs (ramucirumab) can prevent their interaction and VEGFRs phosphorylation/activation [10]. Moreover, a soluble fusion protein which combines ligand-binding elements taken from the extracellular components of VEGFR1 and VEGFR2 fused to the Fc portion of IgG, aflibercept, can mimic VEGFR and trap circulating VEGF [11]. Most other angiogenesis inhibitors, including the

wide family of tyrosine kinase inhibitors, among which sorafenib and sunitinib, inhibit VEGFR tyrosine kinase activity and the downstream signaling pathways, blocking angiogenesis [12,13]. All these antiangiogenic agents are now employed in clinical treatment of cancer patients, alone or combined with conventional chemotherapeutic cytotoxic agents [14]. However, protein drugs, including antibodies, with good target specificity are of high production cost and low metabolic stability. Conversely, small tyrosine kinase inhibitors have low target specificity. Thus, synthetic chemically modified peptides become more and more attractive, because they show better bioavailability and metabolic stability than proteins and better target specificity than small molecules [15-17]. To develop peptide antagonists, two strategies have been adopted so far, the first one is to rationally design peptides based on protein structures and the second one is based on the screening of randomly expressed or synthesized peptide libraries. In our study, we adopted the first strategy to design VEGFRs antagonists by mimicking VEGF receptor binding epitopes conformations.

VEGFR1 and VEGFR2 are structurally related homologues, consisting of seven extracellular ligand binding Immunoglobulin (Ig)-like domains (D1-D7), a transmembrane domain and a cytoplasmic domain, including a tyrosine kinase domain [18]. The X-ray structure of the complex between VEGF dimer and the domain 2 of VEGFR1, VEGFR1-D2 (PDB accession number: 1FLT), shows that VEGF interaction interface is defined by a discontinuous surface [19]. The binding residues belong to three regions of both VEGF monomers: The N-terminal helix (α1), the loop joining the strands β3 and β4 (Loop 2, as indicated in Figure 1) of one VEGF monomer and the loop encompassing β5 and β6 strands (Loop 3, as indicated in Figure 1) of the second VEGF monomer (Figure 1). With respect to VEGFR1-D2, the VEGF binding residues are situated at the bottom of C-end comprising of βa', βc, α-turn between βe-βf, βf and βg strands (Figure 1). Later in 2017, S. Markovic-Mueller *et al*. solved the structure of

the complex formed between VEGF-A and the complete extracellular domain of the receptor VEGFR1 [20]. They showed that VEGF-A binds not only to the VEGFR1-D2, but also to VEGFR1-D3. While the α1-helix binds only to D2, the α2-β2 loop (Loop 1, as indicated in Figure 1) binds to D3, Loop 2 and Loop 3 bind both to D2 and D3. In the structure of the complex, VEGFR1 D2 and D3 domains bind to VEGF-A with similar interface area.

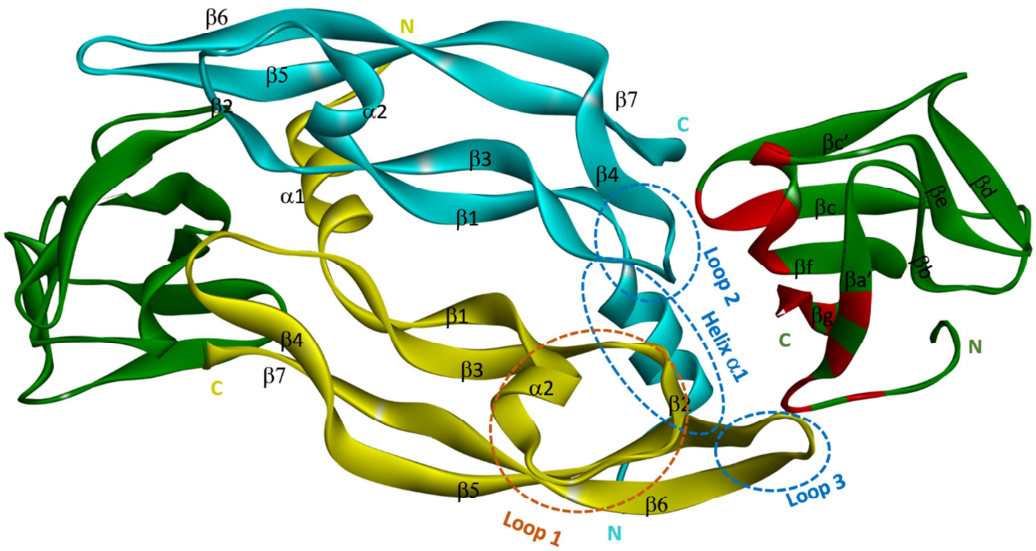

Figure 1: Co-crystalized structure of VEGF-A homodimer (blue and gold) in interaction with two VEGFR1-D2 (green) [19]. The region of one VEGFR1-D2 involved in interaction with VEGF-A is in red. Both VEGFR1-D2 interact with VEGF-A dimer in the same manner. The regions of VEGF-A dimer in interaction with VEGFR1 are circled, among them, Loop 1 (circled in brown dash line) interacts with VEGFR1-D3 (not shown).

Several groups of researchers, including us, have developed conformational constrained peptides reproducing the α1-helix [21-23] the hairpin β5-β6 (Loop 3) [24-27] or the loop β3-β4 (Loop 2) [28-30] of VEGF regions involved in VEGFRs binding. Such constrained

peptides can modulate VEGF biological response. Recently, our group has also reported that cyclic peptides reproducing the loop connecting α2 -β2 (Loop 1) of VEGF were effective in VEGFR1 binding, probably through the interaction with VEGFR1-D3 [31]. On the other hand, peptides mimicking VEGFR1-D2 have also been developed for VEGF binding [32-34].

Although a variety of peptides have been developed by several groups, only few structural binding data are available. In 2010, D'Andrea's group reported the expression and characterization of the uniformly ^{15}N labeled D2 domain of VEGFR1 (^{15}N-VEGFR1-D2) [35]. The interaction between ^{15}N-VEGFR1-D2 and three cyclic peptides, two derived from Loop 2 and the other mimicking the α1 helix of VEGF, has been studied by nuclear magnetic resonance (NMR) [29,36]. However, the cyclic peptides derived from Loop 2 [28,29] could be contaminated by traces of metal catalyst since their synthesis utilized palladium (Pd°) for functional group deprotection before cyclization. We have discovered later that divalent metals can trigger VEGFR1-D2 dimerization [37]. Thus, we firstly optimized the synthetic method without using metal catalyst. The solid phase peptide synthesis and solution phase cyclisation minimized also N-terminal guanidinylation described in the previous synthesis. At the same time, we improved the affinity of cyclic peptides able to bind VEGFR1 by C-terminal substitution [30].

In this paper, we describe the structural studies of the binding to VEGFR1-D2 of one of these C-terminal substituted cyclic peptides (Peptide **3**, Peptide **16** in the previous article [30]) (Figure 2). Firstly, 2D NMR experiments of Peptide **3** alone were performed, then docking studies of the peptide structure on VEGFR1-D2 were carried out. Finally, Single Transition-to-Single Transition Polarization Transfer (ST2-PT) in [^{1}H, ^{15}N]-TROSY [38] two-dimensional on the uniformly ^{15}N labeled VEGFR1-D2 in the absence or presence of the binding peptide were realized. The K_d value of the interaction was also estimated by NMR.

The anti-angiogenic properties of Peptide **3** were evaluated by microtube formation on Matrigel of retinal cell type RF6/A (rhesus macaque choroid-retinal endothelial cells) and of vascular endothelial cell type HUVEC (human umbilical vein endothelial cells) for potential retinopathies and cancer treatment. Several new cyclic peptides, derivatives of Peptide **3**, were also synthesized and their structure-activity relationship was studied by ELISA displacement tests.

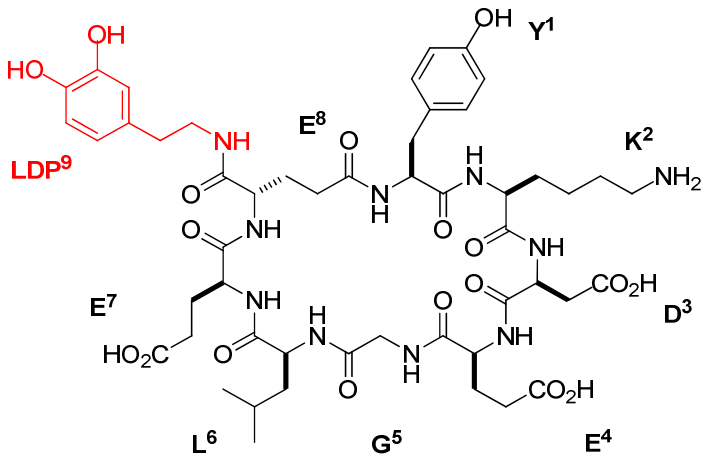

Peptide **3**

Figure 2. Chemical structure of cyclic Peptide **3** (Peptide **16** in the previous article [30]). The residues of amino acids were numbered, the cyclisation between Y^1 and the side chain of E^8 was shown in brackets in Table 1.

2. RESULTS AND DISCUSSION

Cyclic peptide [YYDEGLEE]-NH_2 (Peptide **1** in Table 1) mimicking simultaneously α1 and L2 has been developed in our laboratory [28]. This peptide was modified by replacing Tyr^2 with a Lys residue, obtaining the [YKDEGLEE]-NH_2 peptide (Peptide **2** in Table 1) which lost somewhat its receptor binding affinity, as described by Gautier *et al* [28]. Starting from this latter peptide, we have reported a series of C-terminal modified cyclic peptides, some of

them showing improved VEGFR1 binding affinity in ELISA displacement test. The peptide [YKDEGLEE]-$NHCH_2CH_2Ph(3,4\text{-}diOH)$, Peptide **3** in Table 1, showed a better affinity with respect to C-terminal unmodified cyclic peptide **2** [30].

Peptide **1**	$[Y^1\underline{Y}^2D^3E^4G^5L^6E^7E^8]\text{-}NH_2$
Peptide **2**	$[Y^1\underline{K}^2D^3E^4G^5L^6E^7E^8]\text{-}NH_2$
Peptide **3**	$[Y^1\underline{K}^2D^3E^4G^5L^6E^7E^8]\text{-}NHCH_2CH_2Ph(3,4\text{-}diOH)^9$

Table 1: Cyclic peptides mimicking VEGF-A binding to VEGFR1 [28-30]. The brackets in the peptide sequences indicate the cyclisation between the main chain of Y^1 and the side chain of E^8.

2.1 NMR study of Peptide 3 in solution

Proton NMR 2D spectrum performed on the cyclic peptide **3** shows overlaps between K^2 and D^3, G^5 and E^7, L^6 and E^8, giving less spreading chemical shifts than those of Peptide **1** [28]. The amide region (Figure 3) is well resolved for amino-acids Y^1, E^4 and C-terminal LDP^9 (LDP: dopamine) between 7.6 and 8.46 ppm, but not for the amino acids K^2, D^3, G^5, L^6, E^7 and E^8. The black cross on Figure 3 showed the proximity between the residues Y^1, E^8 and LDP^9, as Peptide **3** was cyclized between the amine group of Y^1 and the side chain carboxylic group of E^8 which carrying the LDP^9 residue at its C-terminal.

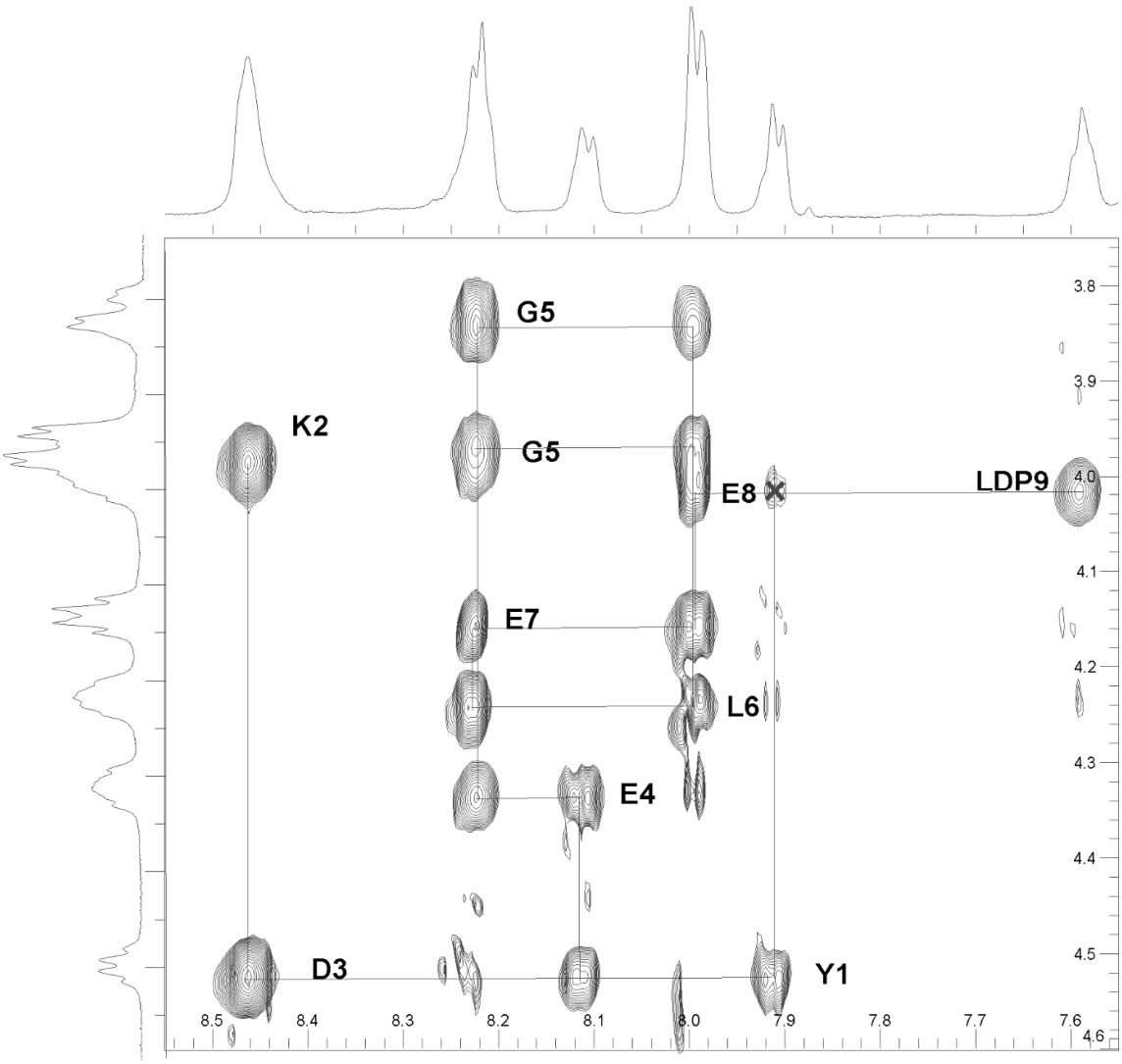

Figure 3: ^{1}H NMR NOESY spectra of the amide region (horizontal spectrum) and the H_{α} (vertical spectrum) of Peptide **3**. The spin systems were identified by 2D TOCSY [39] and DQF-COSY [40] experiments and were sequentially correlated across space thanks to the 2D NOESY experiment [41].

Intraresidual and sequential connectivities were identified for all residues of Peptide **3.** TOCSY [39] and DQF-COSY [40] experiments were used for spin system identification.

NOESY [41] experiment was used for sequential and long-range assignments. 88 NOE restraints were identified on Peptide **3,** of which 59 are intraresidual and 29 sequential. No medium range NOEs ($|i-j| \leq 4$) were observed. Cyclic peptide **3** seems to be less rigid than Peptide **1**, the latter showed one medium range NOE ($|i-j| \leq 4$) on its NOESY spectra [28]. Ramachandran plot analysis shows that Φ/Ψ angles are found in additional allowed region (100%) for Peptide **3**, while for Peptide **1**, indeed Φ/Ψ angles are found in most favoured regions (38%) and residues in additional allowed regions (42%) [28].

Based on data obtained from TOCSY, DQF-COSY and NOESY experiments, the 3D structure calculation was performed using the program X-PLOR [42]. The X-PLOR software, originally developed by Axel Brünger, is now being developed by Ad Bax group at the NIH. This program makes it possible to integrate NMR data such as distances, dihedral angles, coupling constants, paramagnetic or dipolar relaxation data or residual coupling. X-PLOR is therefore particularly well suited to the calculation of structures from NMR data. Ten structures of low calculated overall energy and weak number of distance restraint violations were selected out of 200 calculated structures. None of these structures exhibited NOE violations greater than 0.2 Å. The two aromatic rings, Tyr^1 (Y^1 of Peptide **3**) and C-terminal residue LDP^9 (formula shown in Figure 2), are flexible and have different orientations. The average structure of Peptide **3** in solution was calculated from the 10 best structures which were then superimposed (Figure 4A). The pairwise rmsd calculated on the ten best structures was evaluated at 0.66 ± 0.21 Å on the backbone atoms from residues 1 to 9. The rmsd calculated on the whole backbone atoms for each structure to the average one was evaluated at 0.64 ± 0.14 Å.

The average structure of Peptide **3** (Figure 4B, in salmon color) was superimposed with that of the original Peptide **1** (Figure 4B, in teal-blue color). In fact, the backbone atoms are well

superimposed between residues 1 to 8 with a rmsd of 1.552 Å. Among the common residues of both peptides, the side chains of Asp^3 and Glu^4 have slightly changed their orientations, while residues Leu^6 and Glu^7 showed obviously different orientations. The comparison between Peptide **3** and Peptide **1** showed that the Lys^2 superimposes well with Tyr^2 in Peptide **1**. In previous NMR studies, replacing the Tyr^1 and Tyr^2 by two homophenylalanine had changed peptide conformation [28]. It appears here that the replacement of Tyr^2 by Lys^2 and the C-terminal alkylation have oriented the structure of the peptide in solution to a more stable conformation. However, according to the Ramachandran plot, cyclized peptides are still flexible and can adopt suitable conformation to interact well their target protein. Thus, to test this hypothesis, the docking of Peptide **3** on VEGFR1-D2 was realized.

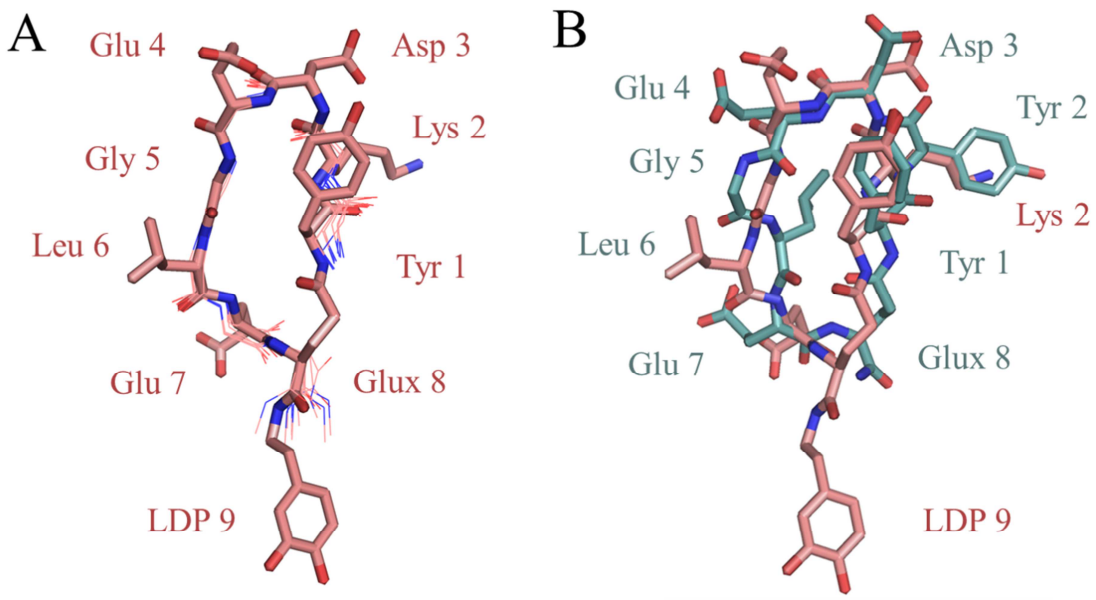

Figure 4: (A) The average structure of Peptide **3** (bold stick in salmon color) obtained by the superimposition of 10 lowest energy structures out of 200 calculated structures. (B) Superimposition of the average structures of peptides **3** (salmon) [28] and **1** (teal-blue).

2.2 Docking of Peptide 3 on VEGFR1-D2

To analyze the peptide receptor binding details, the complex of Peptide **3** in interaction with VEGFR1-D2 was built with the X-PLOR program based on the VEGFR1-D2 structure solved by NMR in the literature (PDB code: 1QSV) [43]. During energy minimization, the average structure of Peptide **3** was used, but not the constraints identified by NMR within Peptide **3**. Atom positions of VEGFR1-D2 were kept fixed and the peptide atoms were free to move. The manual docking started with a structure determined by NMR and the side chains of peptide were free to adapt to the receptor during the formation of the complex. The model of the complex thus obtained by docking shows that Peptide **3** binds to the surface of VEGFR1-D2 comprising the loop βc-βc', the turn between βe-βf and βg (Figure 5C). The structures of the free peptide in solution as determined by NMR and in complex with the receptor after docking were quite similar and the rmsd between the free and the bound peptide was calculated to 0.14 Å.

In the VEGF/VEGFR1-D2 crystalized structure [19], the Cys^{61}-Cys^{68} (Loop 2) fragment of VEGF interacts with VEGFR1-D2 through 2 H-bonds, between the Asp^{63} side chain of VEGF-A and the residue R^{224} of VEGFR1-D2 (Figure 5A). Peptide **1** has 3 H-bonds between the side chains of Asp^{3}, Glu^{4} and Glu^{7} and residues K^{171}, H^{223} and R^{224} of VEGFR1-D2, respectively [29] (Figure 5B). Peptide **3** has different H-bond interaction network. One H-bond between the C-terminal NH of LDP^{9} and the side chain CO of D^{175} of VEGFR1-D2, one between the side chain of Lys^{2} and the backbone CO of T^{222}, one between the backbone CO of Asp^{3} and the side chain of R^{224} and one between the side chain CO of Asp^{3} and the

backbone NH of R^{224}. As already observed in the previous reports [28,29], peptide cyclization or residue variation modify peptide's H-bond network. Besides the H-bond interactions, hydrophobic interactions were expected induced by the C-terminal aromatic ring of Peptide **3** with the hydrophobic residues L^{174} and L^{177} close to D^{175}.

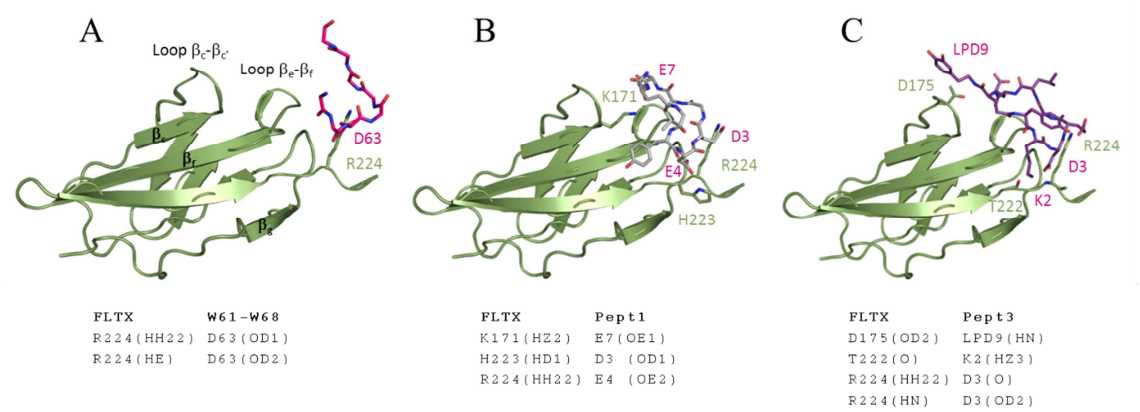

Figure 5: (A) Loop 2 of VEGF (Cys^{61}-Cys^{68}) in the crystallographic complex with VEGFR1-D2 (FLTX): two H-bonds were determined [19]. (B) Theoretical structure of the complex between Peptide **1** and VEGFR1-D2 after docking and minimization with XPLOR: three H-bonds were determined. (C) Theoretical structure of the complex between Peptide **3** (and VEGFR1-D2 after docking and minimization with XPLOR: four H-bonds were determined.

The convergence of the structures is similar for Peptide **1** and for Peptide **3** (Table S1 in supporting information) with a slightly better value for Peptide **1** that could be explained by greater flexibility of Peptide **3.**

The docking experiments showed that Peptide **3** binds to several regions of VEGFR1-D2 identified in complex with VEGF (loop βc-βc', turn between βe-βf and βg) (Figure 5C)

[19,43]. Further structural studies were then conducted by NMR to confirm the ligand-receptor interaction, using the ^{15}N labeled VEGFR1-D2 [35].

2.3 NMR mapping of the interaction between Peptide 3 and VEGFR1-D2

A progressive variation of the ^{1}H and ^{15}N chemical shifts of several signals of the 2D ^{1}H-^{15}N HSQC spectra of VEGFR1-D2 was observed (Figure 6) upon progressive addition of 0 to 8 equivalents of the unlabeled Peptide **3** to ^{15}N-VEGFR1-D2 (260 µM in 50 mM Tris buffer, 150 mM NaCl and pH = 7.2).

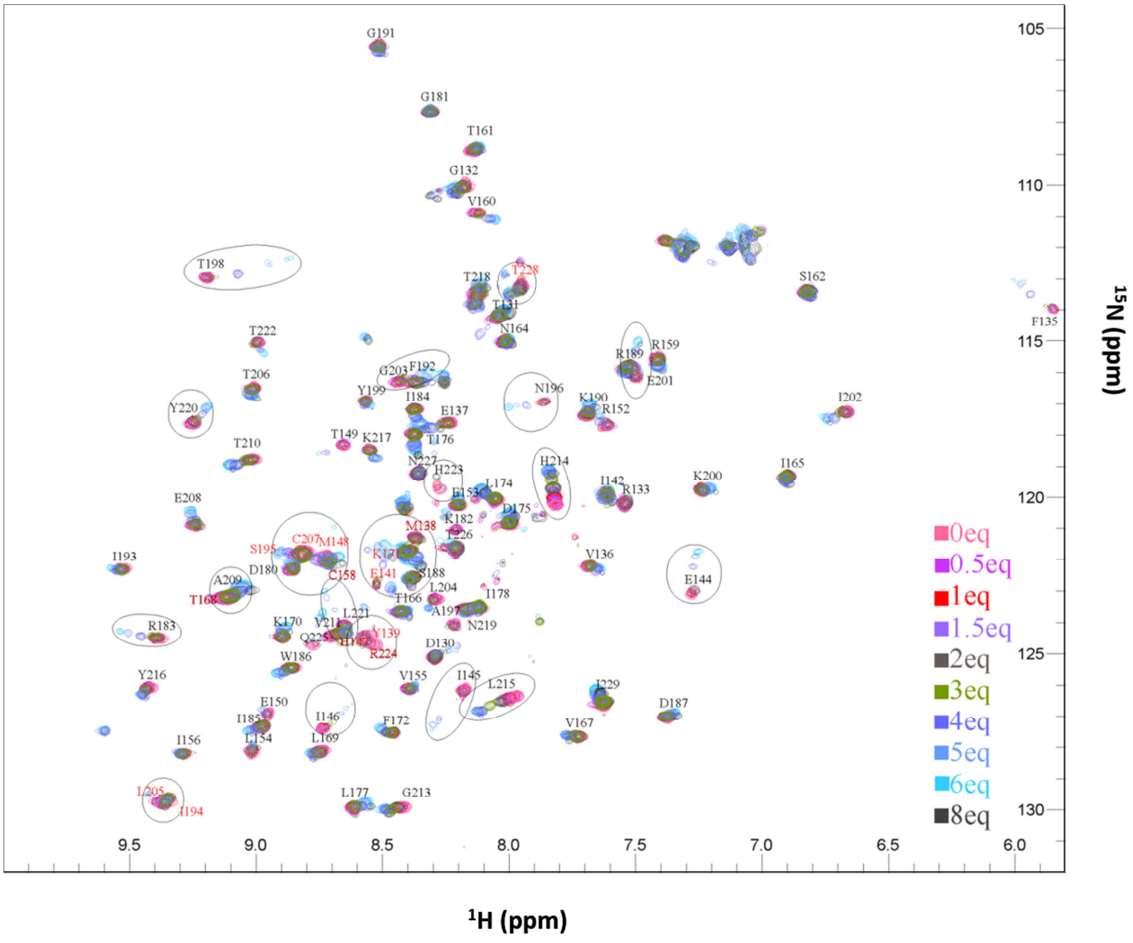

Figure 6: Overlay of [^{1}H, ^{15}N] HSQC spectra of ^{15}N-VEGFR1-D2 (260 µM) with increasing amount of Peptide **3** (0 to 8 eq). The regions of VEGFR1-D2 in interaction with Peptide **3** were identified according the chemical shift perturbation of the ^{1}H and ^{15}N resonances of amino acids involved in the interaction.

VEGFR1-D2 residues having their chemical shifts perturbation ($\Delta\delta HN_{av}$ > 0.1 ppm), under Peptide **3** addition were identified. The $\Delta\delta HN_{av}$ were calculated for the amide ^{15}N and ^{1}H resonances using the equation $\Delta\delta HN_{av}$ (ppm) = $[(0.101* \Delta\delta N)^2 + (\Delta\delta HN)^2]^{1/2}$ where $\Delta\delta N$ and $\Delta\delta HN$ represent the differences between free and bound chemical shifts [44] (Figure S1**,** supporting information). The normalized chemical shifts ($\Delta\delta HN_{av}$) variation of amide NH and ^{15}N within ^{15}N-VEGFR1-D2 at 1, 4 and 8 equivalents of Peptide **3** were shown in Figure **7**.

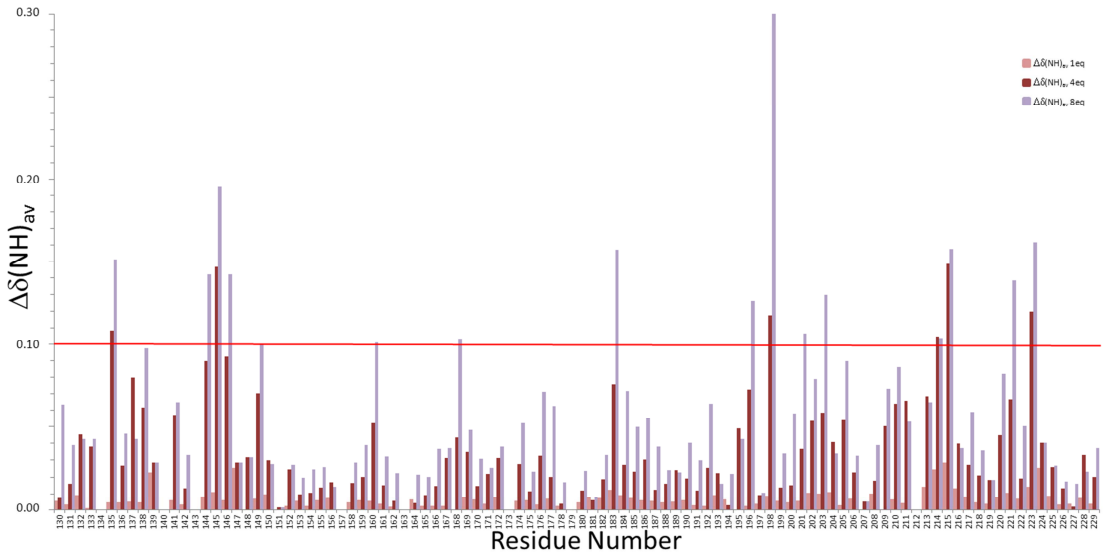

Figure 7: Histograms of the normalized chemical shifts ($\Delta\delta HN_{av}$) variation of amide NH and ^{15}N within ^{15}N-VEGFR1-D2 at 1, 4 and 8 equivalents of Peptide **3**, using the equation $\Delta\delta HN_{av}$ (ppm) = $[(0.101* \Delta\delta N)^2 + (\Delta\delta HN)^2]^{1/2}$ [44].

These residues include E^{144}, I^{145}, I^{146}, T^{149} (βa'), R^{183} (βd), N^{196}, T^{198}, E^{201} (βe-turn-βf), G^{203} (βf), L^{221}, H^{223} (βg). The mapping of the disturbed residues on VEGFR1-D2 structure resolved by NMR (PDB code: 1QSV) [43] showed two separate zones. The first one composed of E^{144}, I^{145}, I^{146}, T^{149}, T^{198}, E^{201}, G^{203}, L^{221}, H^{223}, and the second one composed of R^{183}, N^{196} (Figure 8A). The N-terminal F^{135} and M^{138} were not selected due to their high mobility in solution [43] and are not exposed in the region mapped by all other residues. R^{224} was neither selected since its chemical shift variations were overlapped with those of Y^{139}. The H^{214} and L^{215} were also excluded since different chemical shift values have been observed in different buffer at different pH [37]. All residues situated on βa', βe-turn-βf and βg are located on the surface of VEGFR1-D2 in contact with VEGF-A, in agreement with the regions identified by co-crystallization of the complex of VEGF/VEGFR1-D2 (PDB code: 1FLT [19]) (Figure 8B). Our results confirm that Peptide **3** does interact with VEGFR1-D2. The results are somewhat different from those obtained with Peptide **1** and its analogue [29], so we conclude that the conformations of this series of cyclic peptides is very sensitive to residue modification and thus their interaction with VEGFR1-D2 is different. Therefore, Lys^2 replacement and C-terminal modification in Peptide **3** could alter the conformation of the peptide, the orientation of its side chains and thus its mode of binding to the receptor.

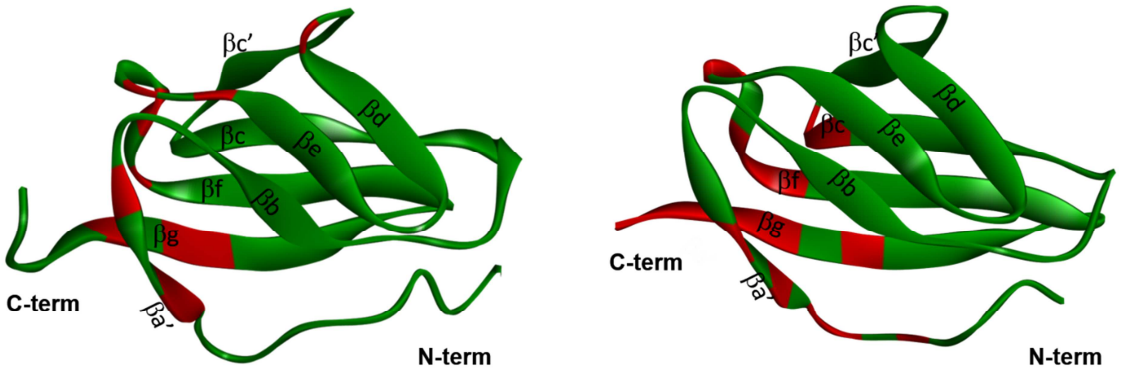

Figure 8: (A). Regions comprising residues of VEGFR1-D2 identified by NMR (E^{144}, I^{145}, I^{146}, T^{149}, T^{198}, E^{201}, G^{203}, L^{221}, H^{223}, R^{183} and N^{196}) by chemical shift perturbation after addition of Peptide **3** are colored in red and mapped on the 3D structure of VEGFR1-D2 resolved by NMR (PDB: 1QSV) [43]. (B). Regions comprising residues of VEGFR1-D2 in interaction with VEGF-A identified by co-crystallization (Y^{139}, E^{141}, I^{142}, P^{143}, I^{145}, H^{147}, K^{171}, F^{172}, P173, Y^{199}, K^{200}, I^{202}, L^{204}, N^{219}, L^{221}, H^{223} and R^{224}) are colored in red (PDB: 1FLT) [19].

The X-ray complex VEGF/VEGFR1-D2 shows two proline residues P^{143} and P^{173} involved in interaction with VEGF-A, but the proline residues cannot be identified in ^{1}H-^{15}N HSQC NMR spectra due to their absence of amide protons. Although the residues of VEGFR1-D2 in interaction with Peptide **3** identified by NMR are not identical to those identified in the VEGF/VEGFR1-D2 co-crystalized complex, they are neighbor residues situated on βa', βe-turn-βf and βg. Since the size of the peptide is much smaller than that of VEGF, it is not surprising that fewer receptor residues were identified during the interaction.

The studies of interactions between Peptide **3** and ^{15}N-VEGFR1-D2 carried out by NMR experiments confirm partially the ligand binding model proposed by molecular docking. The docking predicts 3 residues (D^{175}, T^{222} and R^{224}) of VEGFR1-D2 having 4 H-bonds with Peptide **3**. ^{1}H-^{15}N HSQC NMR spectra of ligand-protein binding identified more residues implied in binding, including 11 residues (E^{144}, I^{145}, I^{146}, T^{149}, R^{183}, N^{196}, T^{198}, E^{201}, G^{203}, L^{221} and H^{223}) having $\Delta\delta HN_{av} > 0.1$ ppm during peptide titration. D^{175} and T^{222} having $\Delta\delta HN_{av} <$ 0.1 ppm were not selected, but they belong to the peptide binding regions. Our results show that Peptide **3** can partly mimic VEGF binding to VEGFR1-D2, but the binding surface on the receptor is limited by the weak molecular size of the peptide. Moreover, Peptide **3** has also much lower affinity than VEGF-A for VEGFR1-D2.

Recently, we have reported that divalent metal ions can induce VEGFR1-D2 dimerization through chelation of residues H^{147} and H^{223} of two VEGFR1-D2 monomers [37]. Homodimeric X-ray structures of VEGFR1-D2 have thus been obtained using Zn^{2+}, Co^{2+} and Cu^{2+} ions. Moreover, the VEGFR1-D2 homodimer interaction surface is composed of an important part of the VEGFR1-ligand binding surface. NMR studies have shown that Cd^{2+} can also induce the dimerization of VEGFR1-D2 in solution. As the previous synthesis of Peptide **1** utilized Pd° [28], it is possible that the observed perturbation of VEGFR1-D2 residues by this peptide may be partly due to traces of metal contamination. In our new synthetic pathway [30], no metal catalyst was used, so we can exclude the effect caused by metal ion in Peptide **3** binding studies.

2.4 NMR determination of K_d of Peptide 3

Although diverse types of peptides have been developed as VEGFR antagonists, few of them have been analyzed in receptor binding structural studies [28,29,45,46]. Only one direct receptor binding affinity has been measured by NMR [36]. Most of the VEGFR antagonist binding assays were based on measuring competitive ability of peptides to displace ^{125}I labeled VEGF to living cell membrane VEGFRs [22,47] or biotin labeled VEGF from the VEGFR [48], or on inhibition of VEGFR1 binding to VEGF-A [49,50]. The NMR titration of the ^{15}N-VEGFR1-D2 by Peptide **3** enables the determination of the dissociation constant K_d for Peptide **3** by evaluating the variation of the ^{1}H and ^{15}N chemical shifts ($\Delta\delta$) of VEGFR1-D2 in the presence of peptide, following equation $\Delta\delta_{calc} = (\Delta\delta max_{av}) / 2 * [B + X - ((B + X)^2 - 4X)^{1/2}]$ where $B = 1 + K_d/[P]_{tot}$, $\Delta\delta max_{av}$ is the normalized chemical shift deviation at saturation, X represents the ratio of the ligand (Peptide **3**) and $[P]_{tot}$ is the total concentration of the protein [51]. Based on different amino acid residues having the coefficient of determination R^2 of 0.7 - 0.8, the K_d was estimated as 621 ± 117 μM (Figure 9).

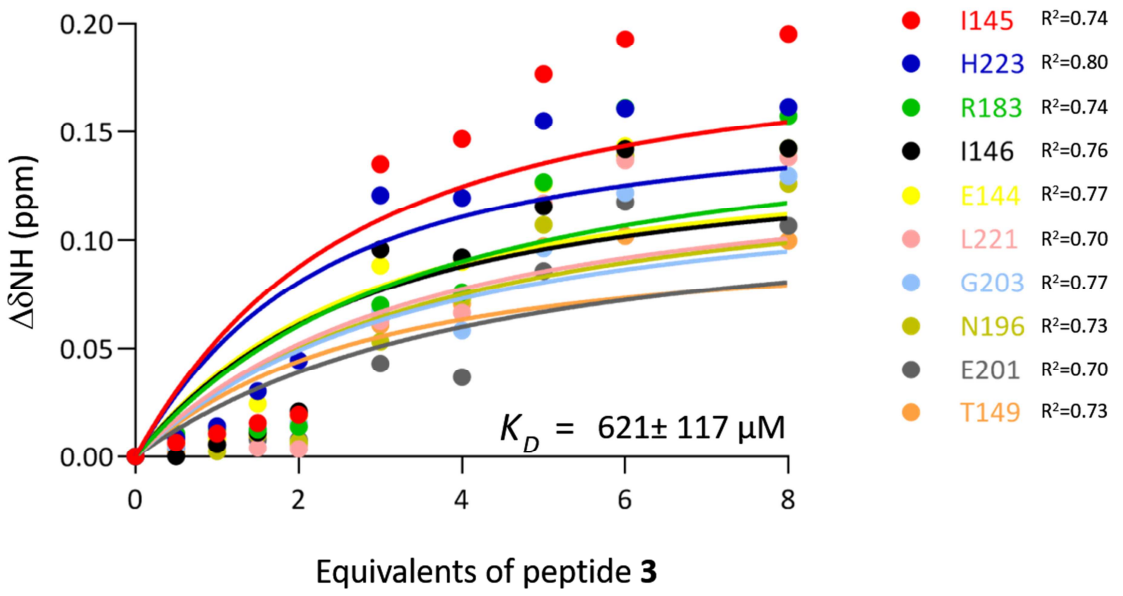

Figure 9: Calculated variation of chemical shift (Δδ) of VEGFR1-D2 residues upon increasing concentration of Peptide **3**. The dots represent the $\Delta\delta HN_{av,}$ where $\Delta\delta HN_{av}$ (ppm) = $[(0.101* \Delta\delta N)^2 + (\Delta\delta HN)^2]^{1/2}$, the solid lines represent fitted curves based on $\Delta\delta_{calc} = (\Delta\delta max_{av}) / 2 * [B + X - ((B + X)^2 - 4X)^{1/2}]$ where $B = 1 + K_d/[P]_{tot}$, $\Delta\delta max_{av}$ is the normalized chemical shift deviation at saturation, X represents the ratio of Peptide **3**/$[P]_{tot}$ and $[P]_{tot}$ is the total concentration of the protein. The curves of the best fit solution of the quadratic function describe a 1:1 complex formation.

The ligand-binding NMR data to its receptor suggest that Peptide **3** could bind to the VEGFR1-D2, on part of the binding surface of VEGF-A, with however low binding affinity. In fact, the recent resolved structure of VEGF-A in interaction with VEGFR1-D2-D7 revealed that the loop β3-β4 (Loop 2) of VEGF-A that we mimicked, mainly interacts through its Asp^{63} (Asp^3 in Peptide **3**) with R^{224} in VEGFR1-D2 and N^{259} in VEGFR1-D3. However, the Glu^{64} of VEGF-A (Glu^4 in Peptide **3**) does not interact with VEGFR1-D2, but with residues R^{261}, R^{280}, Q^{284} and N^{290} in VEGFR1-D3 [20]. Thus, the designed peptides **1** and **3** might

interact not only with VEGFR1-D2 but also with VEGFR1-D3 which cannot be observed in our NMR experiments with VEGFR1-D2.

2.5 Inhibition of $VEGF_{165}$ induced capillary tube formation on Matrigel.

The anti-angiogenic effect of Peptide **3** was evaluated by its ability to inhibit microtube formation of endothelial cells on Matrigel. As pathological angiogenesis is observed in retinopathies and in tumor development, two cell lines were used, one of retinal angiogenesis (cell line RF6/A, rhesus macaque choroid-retinal endothelial cell) and the other of classical vascular angiogenesis (cell line HUVEC, human umbilical vein endothelial cell).

The capillary tube formation of RF6/A cells and HUVEC on Matrigel were induced by VEGF-A (30 ng/mL). At 50 µM, Peptide **3** inhibits effectively the microtube formation of both cell lines on Matrigel. Tube like structures were quantified by manual counting and presented as the percentage of control (without VEGF) (Figure 10A and 10B).

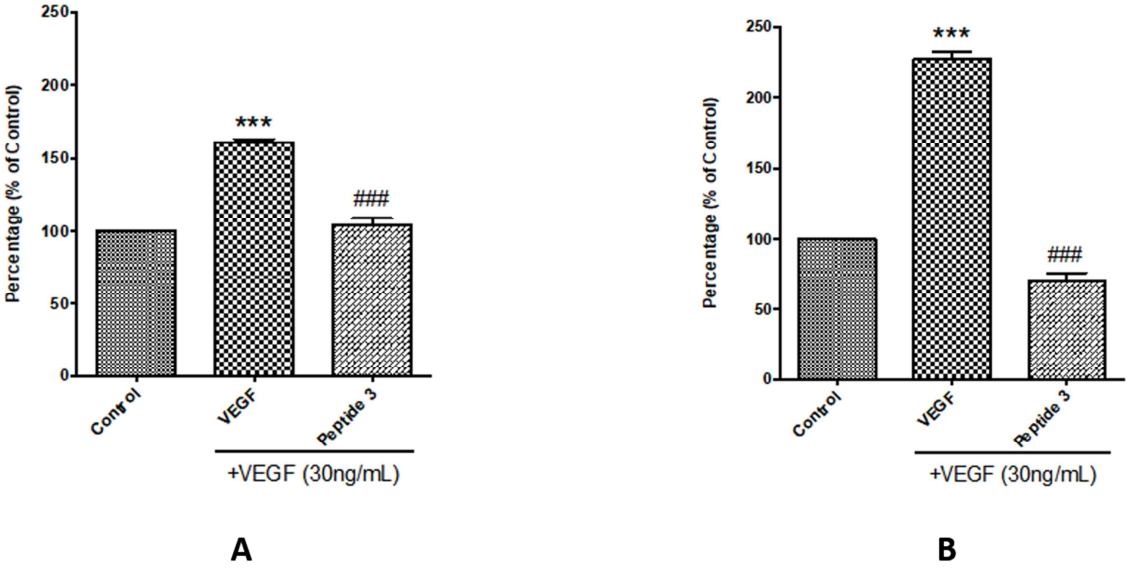

Figure 10: Peptide **3** (50 µM) reduced VEGF-induced tube formation in RF6/A cell (A) and HUVEC (B). Tube like structures were quantified by manual counting and presented as the percentage of control (without VEGF) (n = 2 for RF6A (A) and n = 3

for HUVEC (B)). Data = Means ± SEM. ***P<0.001 versus control, ###P<0.001 versus VEGF.

2.6 New analogues of Peptide 3

Cyclic peptide [YYDEGLEE]-NH_2 (Peptide **1**) has been designed to mimic simultaneously α1 and Loop 2 regions of VEGF [28]. With the aim to label this Peptide **1**, its Tyr^2 was replaced by Lys, leading to Peptide **2** [YKDEGLEE]-NH_2. Lys residue created a potential labeling site but conferred to the peptide a decreased receptor binding affinity [29]. Starting from Peptide **2**, with the aim to perform a new peptide tag for cell imaging study, we designed and synthesized a series of C-terminal modified cyclic peptides, some of which showed an increased binding affinity in ELISA displacement test [30].

Peptide **3** had shown improved affinity compared to Peptide **2**. As the original Peptide **1** showed better receptor binding affinity than Tyr/Lys replacement in Peptide **2**, we replace back the Lys^2 by Tyr^2 to obtain Peptides **4** and by homoPhe to obtain Peptide **5** to investigate the effect of aromatic ring at this position (Table 2). Moreover, docking study of Peptide **1** on VEGFR1-D2 showed that the cycle size is smaller than that of L2 fragment (^{61}CNDEGLEC^{68}) in the complex of VEGF-A/VEGFR1-D2, so an Asn residue of VEGF-A L2 was inserted between Tyr^2 and Asp^3 of Peptide **3**, generating Peptide **6** (Table 2).

All peptides, including the new peptides **4**, **5**, and **6** in Table 2 were synthesized as previously described, without using metal catalyst [30].

Peptide	Sequence	Displacement 100 µM (%)
1	[YYDEGLEE]-NH_2	19.3 ± 4.7
2	[YKDEGLEE]-NH_2	14.5 ± 2.7
3	[YKDEGLEE]-$NHCH_2CH_2Ph(3,4\text{-}diOH)$	48.4 ± 4.8
4	[YYDEGLEE]-$NHCH_2CH_2Ph(3,4\text{-}diOH)$	50.0 ± 1.4
5	[YhFDEGLEE]-$NHCH_2CH_2Ph(3,4\text{-}diOH)$	15.4 ± 2.6
6	[YYNDEGLEE]-$NHCH_2CH_2Ph(3,4\text{-}diOH)$	24.7 ± 2.5

Table 2: Sequence of cyclic peptides used in ELISA and their inhibitory potency. Displacement represents the percentage of btVEGF displaced by the peptides at 100 µM. The values are reported as the average of tests performed each in triplicate.

2.7 ELISA VEGFR1 binding assay

The peptides were evaluated at 100 µM for their capacity to displace biotinylated VEGF-A (btVEGF) from VEGFR1 by an ELISA assay [48]. The results were reported in Table 2. Displacement represents the percentage of btVEGF displaced by peptides at the concentration of 100 µM. As we have already reported, Peptide **3** showed improved affinity compared to Peptide **2** [30] (Table 2). When we replaced again the Lys^2 residue with Tyr^2, the C-end modified Peptide **4** also showed an improvement over the unmodified Peptide **1**. We concluded that in the series of C-end modified peptides, an aromatic ring at position 2 (Tyr^2) is not important for receptor binding. However, the replacement of Lys^2 by homophenylalanine (hPhe or hF) (Peptide **5**), which has been used in previous structure-activity studies of the original peptide [28], provokes the loss of affinity. We supposed that a residue at this position does not necessarily need a side chain with an aromatic ring but with a function that can establish favorable ionic or hydrogen bond interaction with the receptor (as it is the case of Tyr or Lys but not of hPhe). Asn insertion at position 6 in Peptide **6** did not

influence obviously the affinity of the cyclic peptide **2**, moreover it decreased peptide's ability to displace VEGF in respect to Peptide **4**. Thus, the larger cycle is not favorable for the receptor binding in this series of peptides.

Peptide **3** remains the most interesting peptide since the C-terminal modification improved its inhibitory potency of the interaction between VEGF and VEGFRs, and the Lys^2 residue can serve as labeling or conjugation site for further modifications, such as chromophore or DOTA conjugates for imaging studies [52], and for small molecules conjugates to improve antagonist activity.

It is extremely important to note here that the commercial btVEGF does not have always the same biotinylation level for different batches and that the number of biotin molecules linked to one VEGF is never determined. The quantity of btVEGF used for each assay must be verified to reach the same signal level (in relative light units). If the VEGF biotinylation level is low, we should introduce more btVEGF (containing unbiotinylated VEGF), which may give a lower peptide inhibition value. That is the reason that Peptide **1** showed 57% and 73% inhibition at 100 µM respectively in two different batch btVEGF [28,29], and Peptide **2** showed 45% and 12% in another two different assays [19,30]. Thus, all the peptides must be compared using the same btVEGF batch, which is the case in this report.

We have also determined the IC_{50} of Peptide **3** by an ELISA displacement assay. The IC_{50} is evaluated as 196.3 ± 35.4 µM (Figure S2 in supporting information), where a total displacement of btVEGF cannot be reached. The problem was also observed by the group of Barker working on an anti-angiogenic peptide derived from tissue inhibitor of metalloproteinases-3 (TIMP-3) capable of binding to VEGFR2-ECD [53]. In their study, incomplete btVEGF displacement has also been observed. The authors suggested that increasing inhibitor concentrations led to non-specific binding of btVEGF to the plate.

3. CONCLUSION

Here we described the structural study of the binding of a cyclic antagonist peptide on VEGFR1-D2. Molecular docking showed that the peptide can have hydrogen-bond interactions with the VEGFR1-D2. In fact, further NMR studies on ^{15}N labeled VEGFR1-D2 showed that the peptide interacts with the receptor overlapping the interaction regions of VEGFR1-D2 recognized by VEGF. The results obtained here together with those previously reported [28-30], allowed to describe a series of peptides able to bind VEGFR1-D2 but slightly different from VEGF in receptor binding. ELISA displacement tests and Matrigel microtube formation assays confirmed the design of this series of cyclic peptides as VEGFR1 antagonists. Peptide **3**, showing a better inhibitory effect than Peptides **1** and **2**, could be more suitable for further biological investigations. It can also be used for the design of chimeric antagonists to improve inhibitory activity by conjugation with small molecules.

4. EXPERIMENTAL SECTION

4.1 NMR spectroscopy

Peptide **3** employed for NMR studies was prepared by dissolving 1 mg of lyophilized peptide in a mixture of H_2O/D_2O/DMSO-d_6 (v/v 80/10/10, 500µL) at a pH of 2.5. NMR experiments were carried out on a Bruker 600 MHz proton spectrometer Avance III. Double quantum filtered spectroscopy, DQF-COSY, total correlated spectroscopy, TOCSY, with a mixing time of 70 ms and Nuclear Overhauser effect spectroscopy, NOESY with a 250 ms mixing time were performed. Two-dimensional spectra were acquired at 293 K, with 2048 real points in t2, a spectral width of 5040 Hz and 512 t1 increments. The transmitter frequency was set to the water signal. The solvent resonance was suppressed by a 1D Excitation Sculpting using 180 water-selective pulses pulse sequence from the Bruker pulse sequence library (zgesgp). A $\pi/6$ phase-shifted sine bell window function was applied, and data were zero filled once prior to Fourier transformation in both dimensions (t1 and t2). The final sizes of the frequency domain matrices were 2048 and 2048 real points in both dimensions. For all experiments, ^1H frequency scale was directly referenced to water. For all experiments, the temperature was controlled externally using a temperature control system (BCU 05 Bruker). All data were processed using Bruker Topspin (v1.3) software (Biospin;Bruker). The data were then analyzed with the spectrum analysis program (CcpNmr Analysis).

4.2 NMR Structure and analysis of Peptide 3

The 3D structure calculations were performed using X-PLOR [42]. Out of 200 calculated structures, 10 were selected according to their low overall energy and their weak number of distance restraint violations. None of the structure exhibited NOE violation greater than 0.2 Å and all of them revealed a good covalent geometry, with no bond or angle violations. The

Ramachandran plot shows that 100 % of the residues are found in the additional allowed regions. The superimposition of the 10 lowest energy structures on their backbone atoms (residues 1-9) shows a good convergence of the structures (Figure 4A). The pairwise and averaged rmsd calculated on the backbone atoms from residues 1 to 9 was evaluated at 0.66 ± 0.21 Å and 0.64 ± 0.14 Å respectively (Table S1 in supporting information).

4.3 Interaction between Peptide 3 and ^{15}N-VEGFR1-D2 and K_d determination

The uniformly labelled ^{15}N-VEGFR1-D2 was expressed, refolded and purified as described [35]. The protein was then prepared at the concentration of 260 µM in 200 µL of 50 mM Tris buffer at pH 7.2 containing 150 mM NaCl and 10% (v/v) D_2O was titrated with a solution of Peptide **3** at the concentration of 26 mM in DMSO-d6. A TROSY ^{1}H-^{15}N experiment was recorded after each addition of Peptide **3**. Chemical shift referencing of the ^{1}H and ^{15}N resonances was performed using previously published assignments [43]. Then we evaluated the chemical shift perturbations of the ^{1}H and ^{15}N resonances on the TROSY spectra of VEGFR1-D2 after each addition of the cyclic peptide **3**.

$\Delta\delta HN_{av}$, the variation in chemical shifts ($\Delta\delta$) of amide NH and ^{15}N within labeled VEGFR1-D2 at different Peptide **3** concentrations, was normalized using the equation below and was reported on the histogram (Figure 7 and Figure S1 in supporting information) and residues having $\Delta\delta HN_{av} \geq 0.1$ ppm were selected.

$\Delta\delta HN_{av}$ (ppm) = $[(0.101 * \Delta\delta N)^2 + (\Delta\delta HN)^2]^{1/2}$ where $\Delta\delta N$ and $\Delta\delta HN$ represent the differences between free and bound chemical shifts, 0.101 is the report of the constant *gamma* characteristic for each isotope [44] for each amino acid at different ratio peptide/protein. The dissociation constant K_d was obtained by nonlinear least square fit of the data of equation:

$\Delta\delta_{calc} = \Delta\delta max_{av} / 2 * [B + X - ((B + X)^2 - 4X)^{1/2}]$ with $B = 1+K_d/[P]_{tot}$ where $\Delta\delta max_{av}$ is the chemical shift change at saturation, X represents the ratio of the ligand (Peptide **3**) and $[P]_{tot}$ the total concentration of the protein [51]. Except T^{198}, which is not represented on Figure 9 because of its R^2 value smaller than 0.7, all fitted curves showed an R^2 values among 0.7 - 0.8.

4.4 Cell line and culture

The monkey choroid-retinal endothelial cells RF/6A (ATCC, Manassas, VA) were cultured in Roswell Park Memorial Institute 1640 medium (RPMI1640) and Dulbecco's modified eagle medium (DMEM) (Invitrogen, Carlsbad, CA) supplemented with 10 % fetal bovine serum (Invitrogen), 100 U/mL penicillin and 100 µg/mL streptomycin (Invitrogen). Cells were incubated in a humidified atmosphere of 5 % CO_2 at 37 °C.

Human umbilical vein endothelial cells (HUVECs) were purchased from ScienCell Research Laboratories, inc. (Carlsbad, CA). HUVECs were cultured in ECM supplemented with 5% (v/v) fetal bovine serum and 1% ECGS, 100 U/mL penicillin and 100 µg/mL streptomycin. Experiments were performed on HUVECs from passage 3 to 6.

4.5 Capillary tube formation assay

Matrigel was thawed at 4 °C overnight. 96 well plates were placed on ice prior to the procedure. Liquid Matrigel (100 µL) was slowly added to each well followed by carefully shaking for even distribution. All the above processes were carried out on ice. Then, the culture plate was incubated at 37 °C with 5 % CO_2 for 1 h. RF/6A cells were starved in RPMI1640 containing 0.1 % BSA for 4 h. HUVECs were starved in ECM containing 0.1 % BSA for 4 h. Cells ($2*10^4$) in 100 µL of medium were treated with or without Peptide **3** (50 µM) for 15 min and then seeded into 96-well plates pre-coated with Matrigel and incubated

with ECM containing 0.1 % BSA with or without 30 ng/mL VEGF-A for 4 h. Images were pictured under the inverted microscope, and tubes forming intact networks were counted in a blind manner. The results were calculated from two independent experiments with three replicates for RF6A cells and three independent experiments with three replicates for HUVEC.

4.6 Peptide synthesis

All Fmoc protected amino acids and peptide synthesis reagents were purchased from Novabiochem (Merck Millipore, Darmstadt, Germany). Other chemical reagents and solvents are from Carlo Erba Reagents (Val de Reuil, France). Peptides were synthesized in solid phase using Fmoc chemistry on microwave assisted CEM-Liberty 1 synthesizer. HPLC analysis was performed on a Shimadzu Prominence LC-20AD HPLC using a Phenomenex Luna C_{18} column (5 µm, 4.6 × 250 mm) with dual UV detection at 214 nm and 254 nm and a linear A-B gradient (A: 0.1 % TFA aqueous; B: 0.09% TFA in 70 % acetonitrile aqueous) at a flow rate of 1 mL/min. Crude peptides were purified on a on Shimadzu semi-preparative HPLC system using an Alltima C_{18} column (5 µm, 10 × 250 mm) at a flow rate of 2 mL/min. The purity of the peptides was verified by analytical HPLC, and the purified peptides were further characterized by MALDI-TOF mass spectrometry on an Applied Biosystems/MDS SCIEX 4800 MALDI TOF Analyzer with α-cyano-4-hydroxycinnamic acid as matrix.

The new peptides **4**, **5**, **6** were synthesized as described previously [30]. The synthesis of linear peptides was conducted on a CEM-Liberty 1 synthesizer with Fmoc chemistry at 0.1 mmol scale, starting from Fmoc-Gly-ClTrt resin (see the sequences in Table 2). The C-terminal modified amino acid was prepared beforehand as Fmoc-Glu-$NHCH_2CH_2$Ph(3,4-diOH) for the introduction to peptidyl resin. The linear peptide was synthesized by N,N'-diisopropylcarbodiimide (DIC)/ethyl (hydroxyimino)cyanoacetate (Oxymapure®) coupling

and 20 % piperidine Fmoc deprotection, then cleaved from resin by treatment with 2 % TFA and 5 % TIPS (triisopropylsilane) in CH_2Cl_2 (10 mL) during 1 h. The suspension was filtered to 10% pyridine methanol solution (4 mL). After solvents evaporation, the residue was triturated with water and the precipitate collected and dried to give the side chain protected linear peptide. Without purification, the cyclisation between the N-terminal NH_2 of Tyr^1 and the side CO_2H of Glu^8 was realized in N,N-dimethylformamide (DMF) by 3 equivalents of DIC and 1-Hydroxy-7-azabenzotriazole (HOAt). The complete cyclization was checked by HPLC and DMF was then removed by evaporation and the residue precipitated in water, washed thoroughly with an aqueous $NaHCO_3$ solution to remove diisopropylurea and HOAt, and dried. The crude cyclic protected peptide was then treated with 50 % TFA in CH_2Cl_2 with 2 % TIPS during 2 h for complete side chain deprotection. After evaporation, the residue was precipitated in ether and collected by centrifugation, then purified by semi-preparative HPLC. The fractions checked by analytical HPLC analysis, were collected and lyophilized. The peptide identity was finally confirmed by MALDI-TOF mass spectrometry analysis. Analytical results are represented in Table 3.

Peptide	Yield (%)	MS found	Rt (minutes)
4	17	$C_{53}H_{67}N_9O_{19}$, 1134.6 $[M+H]^+$	18.3 (20%–80% B in 30 min)
5	15	$C_{54}H_{69}N_9O_{18}$, 1132.6 $[M+H]^+$	16.2 (30%–100% B in 30 min)
6	13	$C_{57}H_{73}N_{11}O_{21}$, 1248.7 $[M+H]^+$	11.8 (30%–100% B in 30 min)

Table 3: Yield is the total yield of linear peptide synthesis and its cyclization. MS is obtained by MALDI-TOF spectrometry. HPLC retention times (Rt) was obtained by the gradient indicated (mobile phases A: 0.1 % TFA aqueous; B: 0.09 % TFA in 70 % acetonitrile aqueous solutions). Peptides numbers refer to Table 2.

4.7 ELISA VEGF-VEGFR1 Binding Inhibition Assay

The 96-well plate was coated with human extracellular domains (ECD) of VEGFR-1 (R&D Systems, Abingdon, UK) in PBS (20 ng/well) overnight at 4 °C. The plate was washed with 200 µL of wash buffer (PBS containing 0.1 % (v/v) Tween 20), three times and treated with 200 µL of blocking buffer (PBS containing 3 % (w/v) BSA) at 37 °C for 2 h, followed by three washes with wash buffer. 50 µL of peptides solution at 200 µM (twice the desired final concentration) in PBS containing 2 % DMSO were added in triplicate wells and the plate was kept at 37 °C for 1 h. A solution of btVEGF-A_{165} (R & D Systems, Abingdon, UK) at twice the desired final concentration (typically 100 pM) in 50 µL PBS was added. After 2 h incubation, the plate was washed four times with wash buffer. 100 µL of Streptavidin-Horseradish Peroxidase (Amersham, Pittsburgh, PA, USA) diluted 1:8000 in PBS were then added to each well to detect the btVEGFA_{165} bound to the ECD of VEGFR1. After 45 min incubation at 37 °C, in the dark, the plate was washed three times with wash buffer. 100 µL of SuperSignal West Pico Chemioluminescent Substrate (Pierce, Rockford, IL, USA) was finally added and the chemiluminescence was quantified with a Perkin Elmer Victor 2 spectrophotometer (Victor Wallac Multilabel reader). The percentages of displacement were calculated by the following formula: $100 \times [1 - (S - NS)/(MS - NS)]$ where S is the signal measured, NS is the nonspecific binding signal defined as the signal measured in the absence of coated receptor on the microplate, and MS is the maximum binding signal obtained with btVEGF-A_{165} without competitor [48].

5. AUTHOR CONTRIBUTIONS

L.W, S.B.[†], M.V. and W.-Q. L. performed peptide synthesis and ELISA test. P.C. and S.B.[§] performed structural studies. R.D.S. and L.D.D. realized protein expression and purification. L.Z. and L.J. realized cellular assays. All authors wrote this paper and have given approval to the final version of the manuscript.

6. ACKNOWLEDGMENTS

This research was supported by the University Paris Descartes, the "Centre National de la Recherche Scientifique" ("Chaire de partenariat" CNRS-UPD to S. Broussy) and the "Agence Nationale de la RechercheANR"DIC (ANR-2010-BLANC-1533-03 and ANR-2015-CE17-0005-04). L. Wang acknowledges the China Scholarship Council for the donation of a scholarship. We thank the group of Prof. D. Sherman for spectrophotometer plate-reader instrument.

7. ABBREVIATIONS USED

BSA, bovine serum albumin; PBS, phosphate-buffered saline; DIEA, N,N-diisopropylethylamine; DIC, N,N'-diisopropylcarbodiimide; DMF, N,N-dimethylformamide; ECM, extracellular matrix; HOAt, 1-Hydroxy-7-azabenzotriazole; Oxyma Pure, ethyl (hydroxyimino)cyanoacetate; TFA, trifluoroacetic acid; TIPS, triisopropylsilane.

8. CONFLICTS OF INTEREST

The authors declare no conflict of interests.

9. REFERENCES

[1] N. Ferrara, H. P. Gerber, J. LeCouter, The biology of VEGF and its receptors, Nat. Med. 9 (2003) 669–676.

[2] P. Carmeliet, Angiogenesis in health and disease, Nat. Med. 9 (2003) 653–660.

[3] D. Bouïs, Y. Kusumanto, C. Meijer, N.H. Mulder, G.A. Hospers, A review on pro- and anti-angiogenic factors as targets of clinical intervention, Pharmacol. Res. 53 (2006) 89-103.

[4] A.K. Olsson, A. Dimberg, J. Kreuger, L. Claesson-Welsh, VEGF receptor signalling - in control of vascular function, Nat. Rev. Mol. Cell Biol. 7 (2006) 359-371.

[5] A.S. Chung, N. Ferrara, Developmental and pathological angiogenesis, Annu. Rev. Cell Dev. Biol. 27 (2011) 563–584.

[6] D.I. Holmes, I. Zachary, The vascular endothelial growth factor (VEGF) family: angiogenic factors in health and disease, Genome Biol. 6 (2005) 209.

[7] L. Claesson-Welsh, VEGF receptor signal transduction – a brief update, Vascular Pharmacol. 86 (2016) 14–17.

[8] G. Hou-Fu, C.W. Vander Kooi, Neuropilin functions as an essential cell surface receptor, J. Biol. Chem. 290 (2015) 29120–29126.

[9] M. Potente, H. Gerhardt, P. Carmeliet, Basic and therapeutic aspects of angiogenesis, Cell 146 (2011) 873-887.

[10] D.-H. Kong, M.R. Kim, J.H. Jang, H.-J. Na, S. Lee, A Review of anti-angiogenic targets for monoclonal antibody cancer therapy, Int. J. Mol. Sci. 18 (2017) 1786.

[11] J. Holash, S. Davis, N. Papadopoulos, S.D. Croll, L. Ho, M. Russell, P. Boland, R. Leidich, D. Hylton, E. Burova, E. Ioffe, T. Huang, C. Radziejewski, K. Bailey, J. P. Fandl, T. Daly, S.J. Wiegand, G.D. Yancopoulos, J.S. Rudge, VEGF-Trap: a VEGF blocker with potent antitumor effects, Proc. Natl. Acad. Sci. U. S. A. 99 (2002) 11393-11398.

[12] S. Faivre, G. Demetri, W. Sargent, E. Raymond, Molecular basis for sunitinib efficacy and future clinical development, Nat. Rev. Drug Discov. 6 (2007) 734-745.

[13] S. Wilhelm, C. Carter, M. Lynch, T. Lowinger, J. Dumas, R.A. Smith, B. Schwartz, R. Simantov, S. Kelley, Discovery and development of sorafenib: a multikinase inhibitor for treating cancer, Nat. Rev. Drug Discov. 5 (2006) 835-844.

[14] N. Ferrara, A.P. Adamis, Ten years of anti-vascular endothelial growth factor therapy, Nat. Rev. Drug Discov. 15 (2016) 385–403.

[15] D.J. Craik, D.P. Fairlie, S. Liras, D. Price, The future of peptide-based drugs, Chem. Biol. Drug Des. 8 (2013) 136-147.

[16] K. Fosgerau, T. Hoffmann, Peptide therapeutics: current status and future directions, Drug Discov. Today 20 (2015) 122-128.

[17] J.L. Lau, M.K. Dunn, Therapeutic peptides: historical perspectives, current development trends, and future directions, Bioorg. Med. Chem. 26 (2018) 2700-2707.

[18] E. Stuttfeld, K. Ballmer-Hofer, Structure and function of VEGF receptors, IUBMB Life 61(2009) 915-922.

[19] C. Wiesmann, G. Fuh, H.W. Christinger, C. Eigenbrot, J.A. Wells, A.M. de Vos, Crystal structure at 1.7 Å resolution of VEGF in complex with domain 2 of the Flt-1 receptor, Cell 91 (1997) 695-704.

[20] S. Markovic-Mueller, E. Stuttfeld, M. Asthanna, T. Weinert, S. Bliven, K.N. Goldies, K. Kisko, G. Capitani, K. Ballmer-Hofer, Structure of the full-length VEGFR-1 extracellular domain in complex with VEGF-A, Structure 25 (2017) 1-12.

[21] A. Basile, A. Del Gatto. D. Diana, R. Di Stasi, A. Falco, M. Festa, A. Rosati, A. Barbieri, R. Franco, C. Arra, C. Pedone, R. Fattorusso, M.C. Turco, L.D. D'Andrea, Characterization of a designed vascular endothelial growth factor receptor antagonist helical peptide with antiangiogenic activity in vivo, J. Med. Chem. 54 (2011) 1391-1400.

[22] M.I. García-Aranda, S. González-López, C.M. Santiveri, N. Gagey-Eilstein, M. Reille-Seroussi, M. Martín-Martínez, N. Inguimbert, M. Vidal, M.T. García-López, M.A. Jiménez, R. González-Muñiz, M.J. Pérez de Vega, Helical peptides from VEGF and Vammin hotspots for modulating the VEGF-VEGFR interaction, Org. Biomol. Chem. 11 (2013) 1896-1905.

[23] E. Assareh, F. Mehrnejad, K. Mansouri, A.R. Esmaeili Rastaghi, H. Naderi-Manesh, S.M. Asghari, A cyclic peptide reproducing the α1 helix of VEGF-B binds to VEGFR-1 and VEGFR-2 and inhibits angiogenesis and tumor growth, Biochem. J. (2019) DOI: 10.1042/BCJ20180823 (in press).

[24] L. Zilberberg, S. Shinkaruk, O. Lequin, B. Rousseau, M. Hagedorn, F. Costa, D. Caronzolo, M. Balke, X. Canron, O. Convert, G. Laïn, K. Gionnet, M. Goncalvès, M. Bayle, L. Bello, G. Chassaing, G. Deleris, A. Bikfalvi, Structure and inhibitory effects on angiogenesis and tumor development of a new vascular endothelial growth inhibitor, J. Biol. Chem. 278 (2003) 35564-35573.

[25] D. Vicari, K.C. Foy, E.M. Liotta, P.T. Kaumaya, Engineered conformation-dependent VEGF peptide mimics are effective in inhibiting VEGF signaling pathways, J. Biol. Chem. 286 (2011) 13612-13625.

[26] D. Diana, A. Basile, L. De Rosa, R. Di Stasi, S. Auriemma, C. Arra, C. Pedone, M.C. Turco, R. Fattorusso, L.D. D'Andrea, β-hairpin peptide targeting VEGF receptors: design, NMR characterization and biological activity, J. Biol. Chem. 268 (2011) 41380-41691.

[27] L. De Rosa, D. Diana, A. Basile, A. Russomanno, C. Isernia, M.C. Turco, R. Fattorusso, L.D. D'Andrea, Design, structural and biological characterization of a VEGF inhibitor β-hairpin-constrained peptide, Eur. J. Med. Chem. 73 (2014) 210-216.

[28] V. Goncalves, B. Gautier, P. Coric, S. Bouaziz, C. Lenoir, C. Garbay, M. Vidal, N. Inguimbert, Rational design, structure, and biological evaluation of cyclic peptides mimicking the vascular endothelial growth factor, J. Med. Chem. 50 (2007) 5135-5146.

[29] B. Gautier, V. Goncalves, D. Diana, R. Di Stasi. F. Teillet, C. Lenoir, F. Huguenot, C. Garbay, R. Fattorusso, L.D. D'Andrea, M. Vidal, N. Inguimbert, Biochemical and structural analysis of the binding determinants of a vascular endothelial growth factor receptor peptidic antagonist, J. Med. Chem. 53 (2010) 4428-4440.

[30] L. Wang, N. Gagey-Eilstein, S. Broussy, M. Reille-Seroussi, F. Huguenot, M. Vidal, W.-Q. Liu, Design and synthesis of C-terminal modified cyclic peptides as VEGFR-1 antagonists, Molecules 19 (2014) 15391-15407.

[31] L. Wang, L. Zhou, M. Reille-Seroussi, N. Gagey-Eilstein, S. Broussy, T. Zhang, L. Ji, M. Vidal, W.-Q. Liu, Identification of peptidic antagonists of vascular endothelial growth factor receptor-1 by scanning the binding epitopes of its ligands, J. Med. Chem. 60 (2017) 6598-6606.

[32] C. Wiesmann, H.W. Christinger, A.G. Cochran, B.C. Cunningham, W.J. Fairbrother, C.J. Keenan, G. Meng, A.M. de Vos, Crystal structure of the complex between VEGF and a receptor-blocking peptide, Biochemistry 37 (1998) 17765-17772.

[33] M. Reille-Seroussi, J.F. Gaucher, C. Desole, N. Gagey-Eilstein, F. Brachet, I. Broutin, M. Vidal, S. Broussy, Vascular endothelial growth factor peptide ligands explored by competition assay and isothermal titration calorimetry, Biochemistry 54 (2015) 5147-5156.

[34] N. Bayó-Puxan, R. Rodríguez-Mias, M. Goldflam, M. Kotev, S. Ciudad, C.J. Hipolito, M. Varese, H. Suga, R. Campos-Olivas, X. Barril, V. Guallar, M. Teixidó, J. García, E. Giralt, Combined use of oligopeptides, fragment libraries, and natural compounds: a comprehensive approach to sample the druggability of vascular endothelial growth factor, ChemMedChem 11 (2016) 928-939.

[35] R. Di Stasi, D. Diana, D. Capasso, R. Palumbo, A. Romanelli, C. Pedone, R. Fattorusso, L.D. D'Andrea, VEGFR1(D2) in drug discovery: expression and molecular characterization, Biopolymers 94 (2010) 800-809.

[36] D. Diana, R. Di Stasi, L. De Rosa, C. Isernia, L.D. D'Andrea, R. Fattorusso, Structural investigation of the VEGF receptor interaction with a helical antagonist peptide, J. Pept. Sci. 19 (2013) 214-219.

[37] J.-F. Gaucher, M. Reille-Seroussi, N. Gagey-Eilstein, S. Broussy, P. Coric, B. Seijo, M.-B. Lascombe, B. Gautier, W.-Q. Liu, F. Huguenot, N. Inguimbert, S. Bouaziz, M. Vidal, I. Broutin, Biophysical studies of the induced dimerization of human VEGF receptor 1 binding domain by divalent metals competing with VEGF-A, PLoS One 11 (2016) e0167755.

[38] K. Pervushin, G. Wider, K. Wuethrich, Single transition-to-single transition polarization transfer (ST2-PT) in [15N,1H]-TROSY, J. Biomol. NMR 12 (1998) 345-348.

[39] J. Cavanagh, M. Rance, Sensitivity improvement in isotropic mixing (TOCSY) experiments, J. Magn. Reson. 88 (1969) 72-85.

[40] M. Rance, O.W. Sorensen, G. Bodenhausen, G. Wagner, R. Ernst, K. Wuthrich, Improved spectral resolution in COSY H-1-NMR spectra of proteins via double quantum filtering, Biochem. Biophys. Res. Commun. 117 (1983) 479-485.

[41] M. Nilges, G.M. Clore, A.M. Gronenborn, Determination of 3-dimensional structures of proteins from interproton distance data by hybrid distance geometry-dynamical simulated annealing calculations, FEBS Lett. 229 (1988) 317-324.

[42] A.T. Brünger, X-PLOR Software Manual, version 3.1; Yale University Press: New haven (1992).

[43] M.A. Starovasnik, H.W. Christinger, C. Wiesmann, M.A. Champe, A.M. de Vos, N.J. Skelton, Solution structure of the VEGF-binding domain of Flt-1: comparison of its free and bound states, J. Mol. Biol. 293 (1999) 531-544.

[44] M.P. Williamson, Using chemical shift perturbation to characterise ligand binding, Prog. Nucl. Magn. Reson. Spectrosc. 73 (2013) 1-16.

[45] L. De Rosa, F. Finetti, D. Diana, R. Di Stasi, S. Auriemma, A. Romanelli, R. Fattorusso, M. Ziche, L. Morbidelli, L.D. D'Andrea, Miniaturizing VEGF: peptides mimicking the discontinuous VEGF receptor-binding site modulate the angiogenic response, Sci. Rep. 6 (2016) 31295.

[46] R. Di Stasi, D. Diana, D. Capasso, S. Di Gaetano, L. De Rosa, V. Celentano, C. Isernia, R. Fattorusso, L.D. D'Andrea, VEGFR recognition interface of a proangiogenic VEGF-mimetic peptide as determined in vitro and in presence of endothelial cells by NMR spectroscopy, Chem. Eur. J. 24 (2018) 11461–11466.

[47] L.D. D'Andrea, G. Iaccarino, R. Fattorusso, D. Sorriento, C. Carannante, D. Capasso, B. Trimarco, C. Pedone, Targeting angiogenesis: structural characterization and biological properties of a de novo engineered VEGF mimicking peptide, Proc. Natl. Acad. Sci. U. S. A. 102 (2005) 14215-14220.

[48] V. Goncalves, B. Gautier, C. Garbay, M. Vidal, N. Inguimbert, Development of a chemiluminescent screening assay for detection of vascular endothelial growth factor receptor 1 ligands, Anal. Biochem. 366 (2007) 108-110.

[49] M. Reille-Seroussi, J.-F. Gaucher, L.-A. Cussac, I. Broutin, M. Vidal, S. Broussy, VEGFR1 domain 2 covalent labeling with horseradish peroxidase: development of a displacement assay on VEGF, Anal. Biochem. 530 (2017) 107-112.

[50] L. Trapiella-Alfonso, S. Broussy, W.-Q. Liu, M. Vidal, E. Lecarpentier, V. Tsatsaris, N. Gagey-Eilstein, Colorimetric immunoassays for the screening and specificity evaluation of molecules disturbing VEGFs/VEGFRs interactions, Anal. Biochem. 544 (2018) 114-120.

[51] Y. Li, Y. Zhang, H. Yan, Kinetic and thermodynamic characterizations of yeast guanylate kinase, J. Biol. Chem. 271 (1996) 45, 28038-28044.

[52] H. Zhu, C. Zhao, F. Liu, L. Wang, J. Feng, Z. Zhou, L. Qu, C. Shou, Z. Yang, Radiolabeling and evaluation of ^{64}Cu-DOTA-F56 peptide targeting vascular endothelial

growth factor receptor 1 in the molecular imaging of gastric cancer, Am. J. Cancer Res. 5 (2015) 3301-3310.

[53] Y.-Y. Chen, N.J. Brown, R. Jones, C.E. Lewis, A.H. Mujamammi, M. Muthana, M.P. Seed, M.D. Barker, A peptide derived from TIMP-3 inhibits multiple angiogenic growth factor receptors and tumour growth and inflammatory arthritis in mice, Angiogenesis 17 (2014) 207–219.

FIGURE CAPTIONS

Figure 1: Co-crystalized structure of VEGF-A homodimer (blue and gold) in interaction with two VEGFR1-D2 (green) [19]. The region of one VEGFR1-D2 involved in interaction with VEGF-A is in red. Both VEGFR1-D2 interact with VEGF-A dimer in the same manner. The regions of VEGF-A dimer in interaction with VEGFR1 are circled, among them, Loop 1 (circled in brown dash line) interacts with VEGFR1-D3 (not shown).

Figure 2. Chemical structure of cyclic Peptide **3** (Peptide **16** in the previous article [30]). The residues of amino acids were numbered, the cyclisation between Y^1 and the side chain of E^8 was shown in brackets in Table 1.

Figure 3: ^{1}H NMR NOESY spectra of the amide region (horizontal spectrum) and the H_α (vertical spectrum) of Peptide **3**. The spin systems were identified by 2D TOCSY [39] and DQF-COSY [40] experiments and were sequentially correlated across space thanks to the 2D NOESY experiment [41].

Figure 4: (A) The average structure of Peptide **3** (bold stick in salmon color) obtained by the superimposition of 10 lowest energy structures out of 200 calculated structures. (B) Superimposition of the average structures of peptides **3** (salmon) [28] and **1** (teal-blue).

Figure 5: (A) Loop 2 of VEGF (Cys^{61}-Cys^{68}) in the crystallographic complex with VEGFR1-D2 (FLTX): two H-bonds were determined [19]. (B) Theoretical structure of the complex between Peptide **1** and VEGFR1-D2 after docking and minimization with XPLOR: three H-bonds were determined. (C) Theoretical structure of the complex between Peptide **3** (and VEGFR1-D2 after docking and minimization with XPLOR: four H-bonds were determined.

Figure 6: Overlay of [^{1}H, ^{15}N] HSQC spectra of ^{15}N-VEGFR1-D2 (260 µM) with increasing amount of Peptide **3** (0 to 8 eq). The regions of VEGFR1-D2 in interaction with Peptide **3** were identified according the chemical shift perturbation of the ^{1}H and ^{15}N resonances of amino acids involved in the interaction.

Figure 7: Histograms of the normalized chemical shifts ($\Delta\delta HN_{av}$) variation of amide NH and ^{15}N within ^{15}N-VEGFR1-D2 at 1, 4 and 8 equivalents of Peptide **3**, using the equation $\Delta\delta HN_{av}$ (ppm) = $[(0.101* \Delta\delta N)^2 + (\Delta\delta HN)^2]^{1/2}$ [44].

Figure 8: (A). Regions comprising residues of VEGFR1-D2 identified by NMR (E^{144}, I^{145}, I^{146}, T^{149}, T^{198}, E^{201}, G^{203}, L^{221}, H^{223}, R^{183} and N^{196}) by chemical shift perturbation after addition of Peptide **3** are colored in red and mapped on the 3D structure of VEGFR1-D2 resolved by NMR (PDB: 1QSV) [43]. (B). Regions comprising residues of VEGFR1-D2 in interaction with VEGF-A identified by co-crystallization (Y^{139}, E^{141}, I^{142}, P^{143}, I^{145}, H^{147}, K^{171}, F^{172}, P173, Y^{199}, K^{200}, I^{202}, L^{204}, N^{219}, L^{221}, H^{223} and R^{224}) are colored in red (PDB: 1FLT) [19].

Figure 9: Calculated variation of chemical shift (Δδ) of VEGFR1-D2 residues upon increasing concentration of Peptide **3**. The dots represent the $\Delta\delta HN_{av,}$ where $\Delta\delta HN_{av}$ (ppm) = $[(0.101* \Delta\delta N)^2 + (\Delta\delta HN)^2]^{1/2}$, the solid lines represent fitted curves based on $\Delta\delta_{calc} = (\Delta\delta max_{av}) / 2 * [B + X - ((B + X)^2 - 4X)^{1/2}]$ where $B = 1 + K_d/[P]_{tot}$, $\Delta\delta max_{av}$ is the normalized chemical shift deviation at saturation, X represents the ratio of Peptide **3**/$[P]_{tot}$ and $[P]_{tot}$ is the total concentration of the protein. The curves of the best fit solution of the quadratic function describe a 1:1 complex formation.

Figure 10: Peptide **3** (50 µM) reduced VEGF-induced tube formation in RF6/A cell (A) and HUVEC (B). Tube like structures were quantified by manual counting and presented as the percentage of control (without VEGF) (n = 2 for RF6A (A) and n = 3 for HUVEC (B)). Data = Means ± SEM. ***P<0.001 versus control, $^{###}$P<0.001 versus VEGF.

Highlights

- Docking of Peptide **3** (a cyclic peptide mimicking VEGF) on VEGFR1-D2.
- K_d measurement by NMR mapping of Peptide **3** interaction with ^{15}N-VEGFR1-D2.
- Cyclic peptides displace VEGF from VEGFR1 in ELISA test.
- Peptide **3** inhibits VEGF induced tube formation of two cell lines on Matrigel®.

Graphical abstract